Gamow-Teller and dipole strength distribution in $^{40}Ca(n,p)^{40}K$ reaction

B. K. Park and J. Rapaport
Department of Physics, Ohio University, Athens, Ohio 45701

J. L. Ullmann, A. G. Ling, and D. S. Sorenson
Los Alamos National Laboratory, Los Alamos, New Mexico 87544

F. P. Brady and J. L. Romero
Department of Physics, University of California, Davis, Davis, California 95616

C. R. Howell and W. Tornow
Department of Physics, Duke University and Triangle Universities Nuclear Laboratory, Durham, North Carolina 27706

C. T. Rönnqvist
Department of Neutron Research, Uppsala University, Uppsala, Sweden
(Received 18 December 1991)

Double differential cross-section angular distributions covering $0° \leq \theta_{lab} \leq 40°$ have been measured for the $^{40}Ca(n,p)^{40}K$ charge exchange reaction. With the white neutron source at LAMPF-WNR, we were able to study not only the angular distribution but also the energy dependence of this charge exchange reaction covering simultaneously incident neutron energies between 60 and 260 MeV. The identification of Gamow-Teller (GT) transitions and $L = 1$ dipole resonance was carried out using a multipole decomposition technique. The empirically deduced GT strength in the $^{40}Ca(n,p)^{40}K$ reaction evaluated up to 15 MeV excitation energy is compared to theoretical values. We have used a simple one-particle–one-hole shell model calculation to study the excitation of the giant dipole resonance and the giant spin-dipole resonance, which are compared with empirical results.

PACS number(s): 25.40.Hs, 27.40.+z

I. INTRODUCTION

We use the nucleon charge exchange reactions for probing the spin and isospin characteristics in nuclei because of their *ability* to filter out the very dominant isoscalar features in scattering reactions and thus to enhance the isovector response. In this paper we report results from the $^{40}Ca(n,p)^{40}K$ reaction, in particular on the distribution of Gamow-Teller (GT) ($\Delta L = 0$, $\Delta S = 1$, $\Delta J = 1$) strength, and the non-spin-flip ($\Delta S = 0$) and spin-flip ($\Delta S = 1$) $L = 1$ dipole resonances which are referred to as the giant dipole (GDR) and giant spin-dipole (GSDR) resonances, respectively.

Although for $T = 0$ targets, as is in this case, the (n,p) and (p,n) results should be similar, the study of the $^{40}Ca(n,p)^{40}K$ reaction has certain advantages over the study of the $^{40}Ca(p,n)^{40}Sc$ reaction at intermediate energies. In particular, the ground state Q value for the (n,p) reaction is -0.53 MeV compared with -15.1 MeV for the (p,n) reaction. Thus, at forward angles we are able to reach lower momentum transfer, q, values with the (n,p) reaction and therefore are more sensitive to locate GT transitions which peak at $q = 0$. Also, the three-body breakup continuum in ^{40}Sc begins at an excitation energy of 0.37 MeV, while in ^{40}K it starts at 7.83 MeV excitation energy. Therefore, the interpretation of the GDR and GSDR should be easier in the (n,p) reaction without a large contribution from the continuum. Results obtained from the present $^{40}Ca(n,p)^{40}K$ data are compared with results from published $^{40}Ca(p,n)^{40}Sc$ data.

In a simple shell model, the ^{40}Ca ground-state wave function is considered to have nucleons filling the $1d_{5/2}, 2s_{1/2}$, and $1d_{3/2}$ subshells, thus no GT strength is predicted. Since the observed [1–3] GT strength in this nucleus is due entirely to particle-hole (p-h) correlations in the target ground-state wave function, empirical studies are important in the comparison with more sophisticated shell model calculations. One such calculation has been reported by Adachi *et al.* [4] using a second-order perturbation theory. These authors split the total Hamiltonian into an unperturbed part H_0 and perturbing interaction V. H_0 is a one-body Hamiltonian with an uncorrelated ground state. It defines the single particle spectrum from which the intermediate 2p-2h states are built. Adachi *et al.* choose V to be Bertsch and Hamamoto [5] interaction to study GT strength in the $^{90}Zr(p,n)$ reaction. This interaction contains central and tensor components which the authors choose to evaluate separately. Within this model, the authors report a large theoretical GT strength in the low excitation energy region ($E_x < 25$ MeV), but they conclude that the major part of the strength lies at higher excitation energies. The present results are compared with this calculation.

Moreover, recently there has been an active interest in determining the occupation probabilities N_{nlj} of nucleon single-particle orbits in ^{40}Ca, from nucleon elastic scattering data, using a dispersive mean field analysis [6, 7]. As indicated by Macfarlane [8], the ground-state occupation probabilities determine the total non-energy-weighted strength such as GT, observed in isovector excitations.

On the experimental side, Chittrakarn *et al.* [1] and Taddeucci *et al.* [2] have reported on the excitation of two $J^\pi = 1^+$ states in ^{40}Sc at $E_x = 2.7$ and 4.3 MeV. In Ref. [2], the authors estimated the GT strength for the transition to the 2.7-MeV state by comparing the forward angle cross sections for the ^{40}Ca$(p,n)^{40}$Sc(2.7 MeV) and the ^{42}Ca$(p,n)^{42}$Sc(0.611 MeV) transitions. The latter one has a GT strength that may be obtained from beta decay values. In addition to these measurements, transitions to a 1^+ ($T = 1$) state at $E_x = 10.32$ MeV in ^{40}Ca have been observed in inelastic electron [9–12] and proton [3] scattering, and in a gamma-ray resonance fluorescence experiment [13].

The GDR and GSDR were recently studied on ^{40}Ca via (p,n), (γ,n), (p,p'), and $(\vec{p},\vec{p}')$ reactions. The GDR and GSDR were identified in the (p,n) data at 45 MeV [14] and 160 MeV [15], respectively. The location of the nonspin resonance was uniquely shown with (γ,n) data [16]. The spin-dipole strength in ^{40}Ca was examined by comparing 500 MeV (p,p') data to 160 MeV (p,n) data with good agreement [17]. In addition, the evidence of spin-dipole strength was observed in the $(\vec{p},\vec{p}')$ spectra at 319 MeV [18].

The differential cross section angular distributions are calculated with the distorted-wave impulse approximation (DWIA) calculations using the code DW81 [19]. In a multipole decomposition analysis, these calculations are used to evaluate the concentration levels of the angular momentum transfers (L) in each excitation bin of the observed spectra. The detailed multipole decomposition technique is described in Refs. [20, 21]. From the multipole decomposition analysis, we are able to identify L transfers 0 through 3 in the excitation energy region below 35 MeV. The extracted $L = 0$ cross sections are used to obtain GT strength which is then compared with that of the ^{40}Ca$(p,n)^{40}$Sc data. In a simple one-particle–one-hole (1p-1h), the shell model code OXBASH [22] is used to generate the one-body density-matrix elements (OBDME) which are then put into DW81 to calculate the angular distributions for the $L = 1$ excitations, i.e., $J^\pi = 0^-$, 1^-, and 2^- states. These $L = 1$ calculations are compared with the $L = 1$ cross sections obtained from the multipole decomposition analysis.

At large angles ($\theta > 15°$) and high energies ($E_n > 150$ MeV), the dominant feature of the observed spectra is a broad *bump* that is identified as the quasifree (QF) scattering peak. We use an interactive Fermi gas model developed by Brieva [23] to evaluate this cross section.

II. EXPERIMENTAL CONSIDERATION

The double differential cross sections were measured in the angular range between 0° and 40° covering the incident neutron energy from 60 to 260 MeV using the WNR white neutron source at LAMPF. When a 7.5-cm-thick tungsten target located at TARGET-4 is struck by 800-MeV protons delivered from the LAMPF linear accelerator, spallation neutrons with a continuous energy distribution are produced. A more detailed description of this facility is presented by Lisowski *et al.* [24]. The $X(n,p)$ experimental setup [25] is located approximately 90 m away from the neutron production target and 15° left of the proton beam line. Two experimental setups were used for this experiment: the "small-angle" setup for measuring the cross sections in $0° \leq \theta_{\rm lab} \leq 14°$, and the "large-angle"" setup for covering the angular range of $10° \leq \theta_{\rm lab} \leq 40°$. The neutron beam was collimated to a size of 10 × 10 cm^2, approximately the dimensions of the targets used in this experiment. A multitarget array similar to the one described by Henderson *et al.* [26] was used. It consisted of four targets separated by four single-plane multiwire proportional counters (MWPC's). In addition, two veto MWPC's were placed in front of the multitarget array to veto charged particles produced in the neutron flight path. The four targets that were simultaneously studied are listed in Table I.

Each $^{\rm nat}$Ca target (see Table I) was enclosed by 0.5 mm stainless steel windows and the volume between the windows was filled with argon gas. The fourth target position was always occupied by a CH_2 target for an absolute cross section normalization. All veto and target chambers were filled with a gas mixture of 70% argon, 30% CO_2, and 0.2% freon to reduce the hydrogen background contribution [27]. Four drift chambers filled with a gas mixture of 65% argon and 35% isobutane were used to obtain information to calculate the scattering angle and to do the tracebacks of charged particles leading to the CsI detectors. In the small-angle setup, a dipole magnet (0.5 T) was used to deflect the forward-scattered charged

TABLE I. Four targets that were studied simultaneously in the "small-angle" and "large-angle" setups. The fourth target position was always occupied by a CH_2 target to allow for an absolute normalization using H(n,p) cross section. The ^{60,64}Ni(n,p) [29] and ^{32}S(n,p) [50] reactions are subjects of other studies.

Target position	"Small-angle" setup	"Large-angle" setup
1	$^{\rm nat}$Ca (200 mg/cm^2, 97% ^{40}Ca, 12.5 × 12.5 cm^2)	$^{\rm nat}$Ca
2	^{60,64}Ni (each 150 mg/cm^2, 7.5 × 5 cm^2) [29]	$^{\rm nat}$Ca
3	$^{\rm nat}$S (200 mg/cm^2, 95% ^{32}S, 12.0 × 12.0 cm^2) [50]	$^{\rm nat}$Ca
4	CH_2 (76.1 mg/cm^2, 12.0 × 12.0 cm^2)	CH_2

particles out of the neutron beam and into the detector array. A large plastic ΔE scintillator (30.5 x 50.8 x 0.5 cm^3) was positioned in front of the CsI(Tl) detectors E to determine the incident neutron energies using the time-of-flight technique as well as to provide particle identifications. The energy of detected protons was measured with 15 CsI crystals (each 8.9 x 8.9 x 15.2 cm^3) that were stacked up in an array of three rows and five columns. For the large-angle setup, the multitarget array was moved downstream closer to the CsI detectors to cover the angular range between 10° and 40°. No dipole magnet was used in this setup. This increased the solid angle as well as the angular range, and provided an overlap with the data obtained between 0° and 14°. The overall energy resolution was 1.0 to 3.0 MeV depending primarily on the values of the incident neutron energy E_n and reaction angle θ. All data were normalized to the ^{1}H(n,p) cross section obtained from the SM88 phase-shift solution of Arndt *et al.* [28].

The multitarget array chambers operated at a level of 93–97% efficiency. Therefore, the excitation spectra for targets 2, 3, and 4 had to be corrected for misidentified events, i.e., events incorrectly associated with a target downstream of the true target. The technique used to correct for misidentified events has been recently reported by Ling *et al.* [29].

It was found at an early stage in the data analysis that the energy resolution of the signal (target-in) histogram

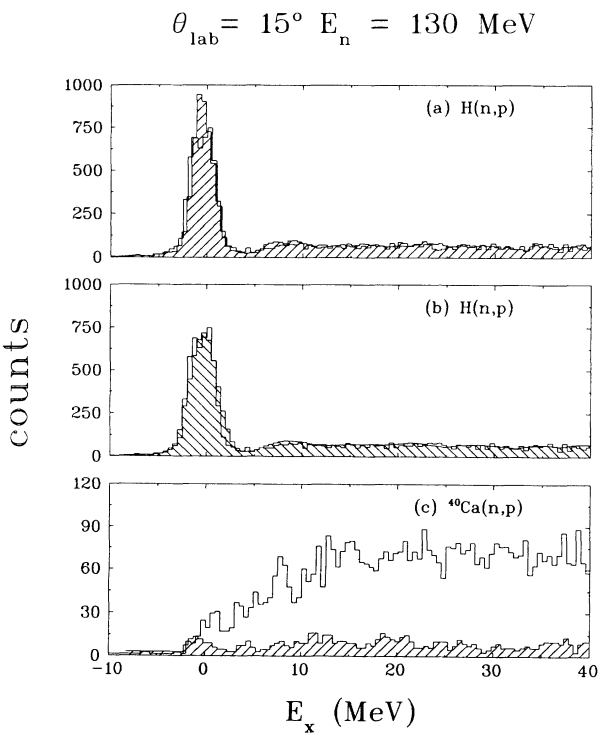

FIG. 1. Background subtracted histograms for the 120 $\leq E_n \leq$ 140 MeV (n,p) data at 14° $\leq \theta_{lab} \leq$ 16°: (a) H(n,p) signal and normalized background in shaded area, (b) H(n,p) signal and blurred-normalized background in shaded area, and (c) ^{40}Ca$(n,p)^{40}$K signal and blurred-normalized background in shaded area.

was different from that of the measured background with empty target to an extent that the difference could not be neglected especially for the data representing the angular region larger than 10°. As can be seen in Fig. 1, the signal histogram has a much broader H(n,p) peak than that of the background histogram. Thus the background was subtracted from the signal histograms after it was blurred. If this blurring is not done, the background subtracted histogram will not only show artificially created peaks but also over/under subtracted peaks. The blurring was done by overlaying a number of identically normalized-background histograms at fixed intervals until the desired resolution was achieved [21].

In the small-angle setup, the required magnetic field resulted in an energy dependent solid angle. The Monte Carlo simulation program GEANT [30] was used to calculate the solid angles. The procedures as well as outputs of GEANT for the present setup are documented in Ref. [21]. For large-angle data that were measured without a dipole magnet, a simple but very effective Monte Carlo simulation code MAGPLT was used [25, 31].

III. RESULTS

In this section, we present the comparisons between the theoretical and experimental work including the techniques and results of a multipole decomposition analysis, and comparisons between the present ^{40}Ca$(n,p)^{40}$K and previous ^{40}Ca$(p,n)^{40}$Sc results at E_p = 134 MeV [1] and E_p = 160 MeV [2]. First, we survey the inputs required for doing the distorted wave impulse approximation (DWIA) calculations using the code DW81: (a) the Franey and Love t-matrix [32] form of the effective free nucleon-nucleon (NN) interaction; (b) Schwandt's phenomenological global optical-model parameters [33] obtained from proton elastic scattering data in the 80 to 180 MeV energy range; (c) harmonic oscillator single-particle wave functions with an oscillator parameter b = 1.94 fm [34]; (d) depending on how the calculations are to be used, the nuclear structure coefficient, Z^J, is estimated accordingly. In the multipole decomposition analysis we have assumed 1p-1h single-particle transitions. Because coefficients of the cross sections for different multipolarities are determined by a least-squares fit method [35], only shapes for the different multipolarities are needed. A second set of DWIA calculations has been carried out in order to find the absolute cross section of a given excited state. The shell model code OXBASH [22] is used to generate the one-body density-matrix elements (OBDME) for the corresponding 1p-1h configurations. The OXBASH calculations are done in the SDPF shell-model space: $1d_{5/2}, 1d_{3/2}, 2s_{1/2}$ holes and $1f_{7/2}, 1f_{5/2}, 2p_{3/2}, 2p_{1/2}$ particles assuming $1\hbar\omega$ excitations. The transition densities are obtained from the calculated wave functions using the Millener and Kurath [36] form of interaction.

For incident neutron energies E_n below 100 MeV we have binned the data in 10-MeV intervals, whereas for E_n greater than 100 MeV we have binned the data in 20-MeV intervals to increase the statistics. For instance, the 130-MeV ^{40}Ca$(n,p)^{40}$K data represent the data between

$120 \leq E_n \leq 140$ MeV. We have done DW81 calculations at $E_n = 95$, 130, and 170 MeV. The choice of $E_n = 95$ and 170 MeV was made to provide *enough* energy separation to be able to observe the energy dependence of the spin-flip and non-spin-flip cross sections. In addition to having comparable energy resolution in both 95- and 170-MeV data, we could use Schwandt's optical-potential parameters which cover the same energy range. As indicated in Ref. [37], there is a strong energy dependence for the ratio of spin transfer to non-spin-transfer charge exchange cross sections in the 60–200 MeV region. Thus, as large an energy separation as possible is preferable to identify these two modes of excitations. However, we have decided on the two energies mentioned above because of the poor statistics for the data in the $E_n > 200$ MeV region.

A. Multipole decomposition analysis

In order to identify the L contributions in each excitation bin, a multipole decomposition analysis [20] was performed. In this approach center-of-mass double differential cross-section data, binned in 1 MeV excitation energy steps, were fitted with DW81 outputs also prepared in 1-MeV energy intervals using a least-squares fit technique. The choice of 1-MeV excitation energy binning was made to have a bin size smaller than the experimental energy resolution in order to distinguish the peaks of interest. At $E_n = 170$ MeV, the observed energy resolution is about 1.5 MeV.

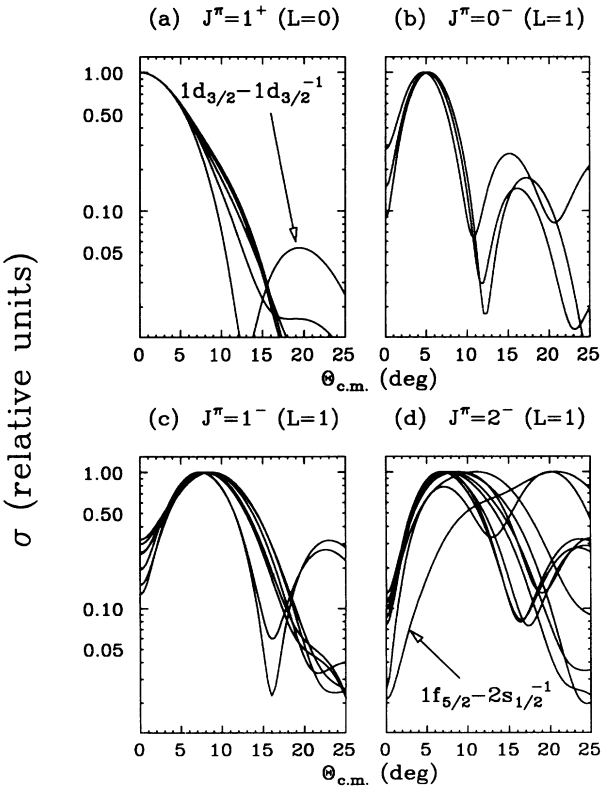

FIG. 2. Arbitrarily normalized DW81 cross-section angular distributions of the $J^\pi = 1^+, 0^-, 1^-$, and 2^- at $E_n = 170$ MeV for the ^{40}Ca$(n,p)^{40}$K reaction.

Since the shapes of the calculated angular distributions are characterized by ΔJ^π transfers, $\sigma(\theta)^{J^\pi}$, all possible 1p-1h configurations for the J^π states $1^+, 0^-, 1^-, 2^-, 2^+, 3^+, 3^-$, and 4^- have been investigated. Some of the DW81 outputs obtained at $E_n = 170$ MeV for these 1p-1h configurations are shown in Fig. 2. The calculated angular distributions in this figure have similar shapes for a given J^π state assuming different p-h configurations. However some exceptions can be found, for example: (1) In Fig. 2(a), it is shown that the $1d_{3/2}1d_{3/2}^{-1}$ p-h configuration for a $\Delta J^\pi = 1^+$ transition has a second maxima at about 20°; we assumed that this p-h configuration may have a large $L = 2$ contribution; (2) the shape for the $\Delta J^\pi = 2^-$, $1f_{5/2}2s_{1/2}^{-1}$ p-h transition peaks at around 20° as can be seen in Fig. 2(d), whereas other 1p-1h configurations for the same ΔJ^π transfer peak at ~7°; again this particular transition may have a large $L = 3$ component.

The strength of each 1p-1h configuration for a transition to a given eigenstate was calculated with the OXBASH shell model code. Based on this calculation, we have chosen the p-h configuration with the largest amplitude to represent each ΔJ^π transition for the multipole decomposition analysis. In Table II, we list the p-h configurations used to represent the respective ΔJ^π transitions in the multipole decomposition analysis. The shape of $\sigma(\theta)$ changes smoothly with increasing excitation energy E_x. Therefore, we have done DW81 calculations in 5 MeV E_x intervals between 0 and 35 MeV, for each p-h configuration representing the J^π state of interest. An interpolation routine is used to supply necessary shapes in steps of 1 MeV.

The shapes of the calculated angular distributions are characterized by ΔJ^π transfers, but the difference in shapes among the members of a given ΔL transfer were not large enough to determine individual ΔJ^π contributions from the present experimental data. Therefore, we prefer to report the results of the multipole decomposition analysis by grouping all ΔJ^π transitions that correspond to a given ΔL transfer. As such we assume $\Delta L = 0$ for the $\Delta J^\pi = 1^+$ transition, ΔL = 1 for ΔJ$^\pi$ = $0^-, 1^-$, and 2^- transitions, $\Delta L = 2$ for $\Delta J^\pi = 2^+$ and 3^+ transitions, and $\Delta L = 3$ for $\Delta J^\pi = 3^-$ and 4^- transitions.

In doing the multipole decomposition analysis, the observed angular distributions for each excitation energy bin are used in the fitting routine. In the present study, cross sections at 10 angles are used between 0° and 20°

TABLE II. The particle-hole configurations used in the multipole decomposition analysis for the ^{40}Ca$(n,p)^{40}$K data.

J^π	p-h	J^π	p-h
0^-	$2p_{1/2}2s_{1/2}^{-1}$	2^+	$2s_{1/2}1d_{5/2}^{-1}$
1^-	$2p_{3/2}1d_{3/2}^{-1}$	3^-	$1f_{7/2}2s_{1/2}^{-1}$
1^+	$2s_{1/2}2s_{1/2}^{-1}$	3^+	$2s_{1/2}1d_{5/2}^{-1}$
2^-	$1f_{7/2}1d_{3/2}^{-1}$	4^-	$1f_{7/2}2s_{1/2}^{-1}$

in 2° steps: 6 angles from the small-angle setup data ($0° \leq \theta_{\rm lab} \leq 12°$) and 4 angles from the large-angle setup data ($12° \leq \theta_{\rm lab} \leq 20°$). Although the small-angle setup data extend out to 14°, the last portion (12° to 14° scattering angle) is not used because of the poor statistics that resulted from a rather small acceptance. It would be ideal to be able to deduce the strength distribution of each ΔJ^π transition listed above. However, χ^2 procedures limit the number of parameters that we can use in fitting 10 cross sections. Therefore, in the present multipole decomposition anaysis, we used a set of five fitting coefficients to describe the experimental data

$$\left(\frac{d\sigma(\theta)}{d\Omega}\right)_{\rm data} = \sum_{J^\pi} \alpha_{J^\pi} \sigma_{J^\pi}^{\rm DW81}(\theta), \quad (1)$$

and the result of doing a least-squares fitting with five coefficients are stored, and the set of coefficients giving the minimum error is chosen out of the positive α coefficients. The positive coefficients ensure that we have positive cross sections.

In Figs. 3, 4, and 5, we show the multipole decomposed spectra for the 95, 130 and 170 MeV ^{40}Ca$(n,p)^{40}$K data at various angles. Since the acceptance was angle, target-position, and E_x dependent, we note that the angles used in the figures presented here are those of median and not weighted angles. In most cases, we work with q rather than θ and therefore the median angles are used only to represent the angle segments from which respective spectra were gathered. The excitation energy spectra ($E_x \leq$ 35 MeV) were decomposed with five $\sigma(\theta)^{J^\pi}$ shapes to represent four multipolarities, namely, $L = 0$, 1, 2, and 3 transfers: 1^+ for $L = 0$ transfer, 1^- and 2^- for $L = 1$ transfer, 3^+ for $L = 2$ transfer, and 4^- for $L = 3$ transfer. These choices of J^π states to *match* the data were done with the overall χ^2—smaller being the obvious choice. The calculated angular distributions for the $J^\pi = 2^+$ and 2^- states were not too different, and the present ^{40}Ca$(n,p)^{40}$K data with less than ideal energy resolution were not sensitive enough to distinguish properly between these two transitions. Thus, the present results for isovector quadrupole strength may not be very reliable. The results of the multipole decomposition analysis are shown in Figs. 3, 4, and 5 for data obtained at 95, 130, and 170 MeV, respectively, and a fairly good agreement is observed with the measured cross sections. Although we estimated all the ΔJ^π transitions mentioned above, the $\Delta J^\pi = 1^+, 1^-, 2^-, 3^+$, and 4^- transitions as

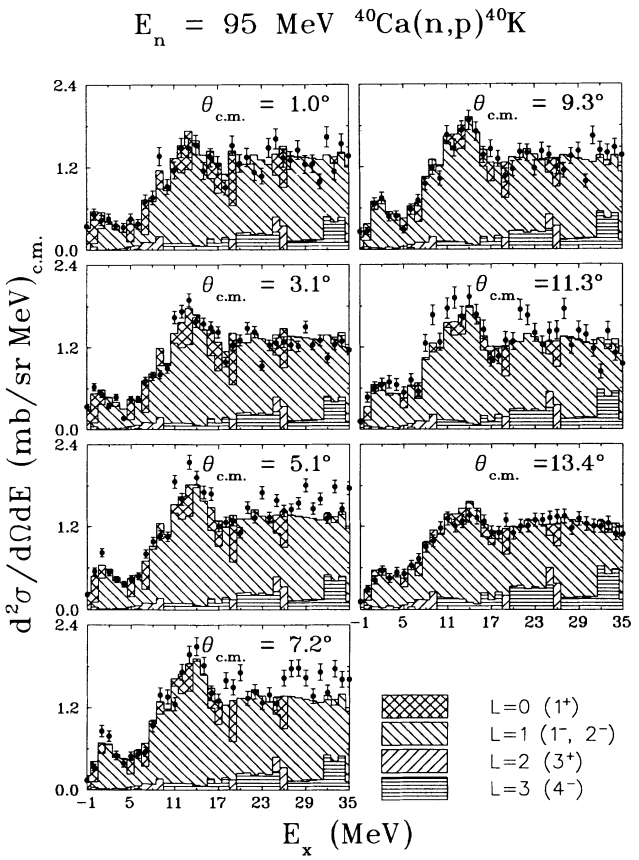

FIG. 3. Multipole decomposed spectra for the 95-MeV ^{40}Ca$(n,p)^{40}$K reaction at various angles. Experimentally observed cross sections are displayed with error bars representing the statistical uncertainties. Cross sections characterizing the L transfers of 0, 1, 2, and 3 are shown. The hydrogen contamination is visible near $E_x \sim 0$ MeV at forward angle spectra.

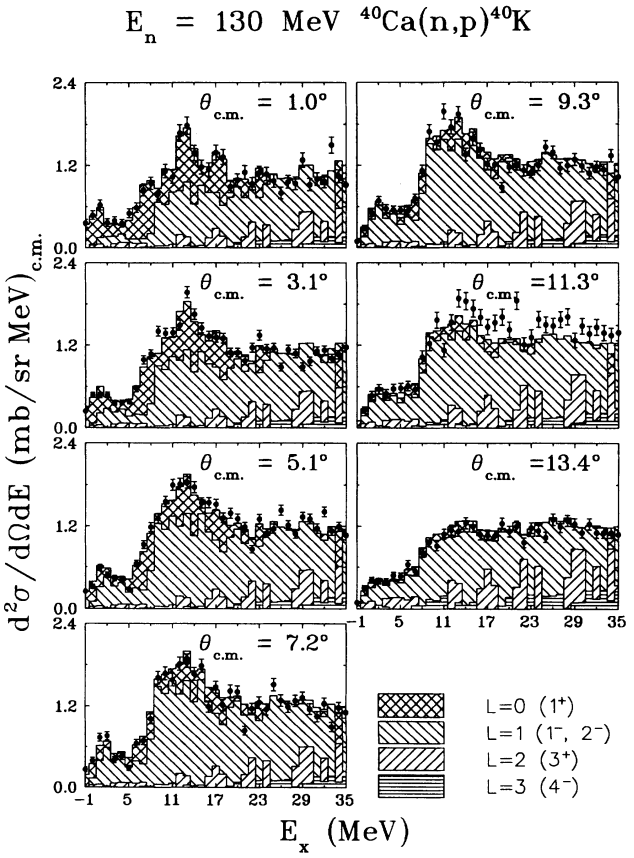

FIG. 4. Multipole decomposed spectra for the 130 MeV ^{40}Ca$(n,p)^{40}$K at various angles. See Fig. 3 caption.

presented in these figures seem to *match* the data reasonably well. We have not included the 0^- contributions to the cross section. Using the results of the 1p-1h shell model analysis, we calculated the 0^- differential cross sections to be rather small. In multipole decomposition analysis, we concluded that its inclusion did not influence the outcome of the fitting. In these spectra, the presence of the 2^- state at $E_x = 0.8$ MeV is more apparent at 170 MeV than 95 MeV, because of its spin-dipole nature. As expected, the cross sections for the quadrupole and octupole states show strong influence at larger angles or momentum transfers. At forward angles and excitation energies below 25 MeV, the differential cross section is dominated by dipole and spin-dipole states.

B. GT transitions

Two $J^\pi = 1^+$ states have been identified in the ^{40}Ca$(p,n)^{40}$Sc reaction. The transition to the lower state at $E_x = 2.7$ MeV in ^{40}Sc has been identified by Taddeucci *et al.* [2] as a GT transition. In order to evaluate the GT strength, the authors compared the cross section to the ^{42}Ca$(p,n)^{42}$Sc(0.61 MeV) cross section measured under the identical experimental conditions. The latter transition is analogous to the ^{42}Ti$(\beta^+)^{42}$Sc(0.61 MeV) beta decay, for which the B(GT) value is known. By taking the ratio of the (p,n) cross sections of the ^{40}Sc(2.7 MeV) and ^{42}Sc(0.61 MeV) transitions, a $B(\mathrm{GT}) = 0.21 \pm 0.04$ was deduced for the transition to ^{40}Sc(2.7 MeV). The unit chosen for B(GT) values in this paper is such that in the decay of the free neutron $B(\mathrm{GT}) = 3$. The authors also *indicated* that a transition to a neutron group located at $E_x = 4.3$ MeV in the ^{40}Ca$(p,n)^{40}$Sc was characterized by an $L = 0$ transfer. However, no B(GT) value was assigned to this transition. The ^{40}Ca$(p,n)^{40}$Sc reaction has also been studied at 134 MeV by Chittrakarn *et al.* [1] who reported that the peak located at 4.3 MeV is primarily a 1^+ state, and that at forward angles it has approximately the same differential cross section as the transition to the 2.7-MeV state. Although the authors of Ref. [1] did not report B(GT) values, for the discussion that follows we assign $B(\mathrm{GT}) = 0.20$ to the transition to a 1^+ state at 4.3 MeV.

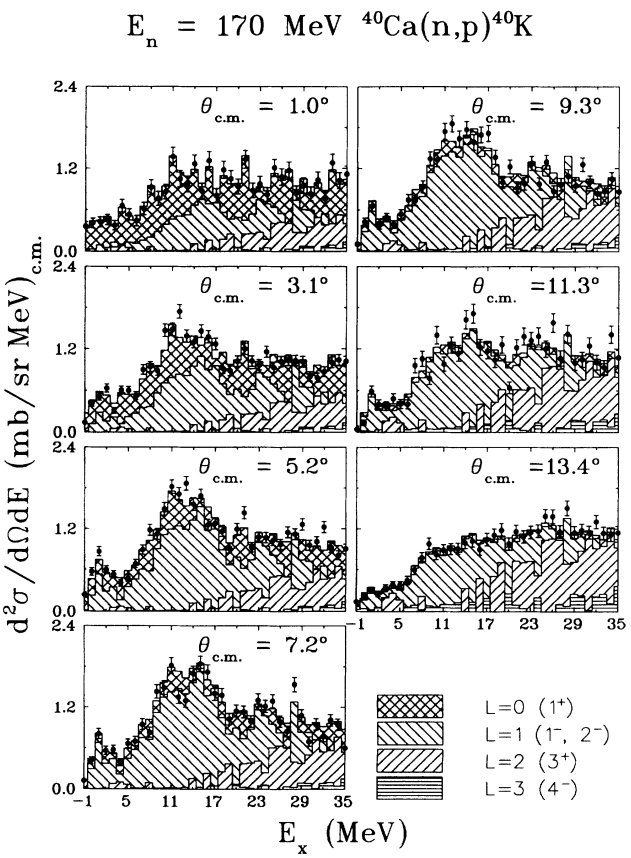

FIG. 5. Multipole decomposed spectra for the 170 MeV ^{40}Ca$(n,p)^{40}$K at various angles. See Fig. 3 caption.

The Ca targets used in this experiment had a hydrogen contamination. As a result we observed a small proton group in the spectra, which follows the kinematics of the H$(n,p)^1$H reaction. With this in mind, we put more confidence on the B(GT) deduced for the group at 4.3 MeV than the one deduced for the group at 2.7 MeV.

We have obtained B(GT) values from the $L = 0$ cross sections deduced from the multipole decomposed spectra. We used the expression

$$B(\mathrm{GT}) = \frac{\sigma_{L=0}(q=\omega=0)}{\hat{\sigma}}, \tag{2}$$

where ω is the energy transfer and the values for the unit cross section $\hat{\sigma}$ were determined from the *universal* relationship

$$\hat{\sigma}(A,E) = 0.1 \times 10^{(1.855+0.00112E-0.08A^{1/3})}. \tag{3}$$

This empirical *universal* relationship was obtained for $X(n,p)$ reactions as a function of E_n for medium mass targets [38], and is valid in the neutron energy region between 70 and 220 MeV. The unit cross section $\hat{\sigma}$ is a proportionality factor that depends on both the nucleus of interest and the incident nucleon energy. The empirical values were obtained by taking the ratio of the $q = 0$ extrapolation of the measured forward angle differential GT cross section and the corresponding GT strength B(GT) known for the corresponding transitions from beta decay measurements. The $\hat{\sigma}(A,E)$ assumed to be a smooth function of mass number A and energy E, represented by Eq. (3), may be used in transitions for which the GT strength is not known.

Using Eq. (3) we calculate $\hat{\sigma} = 5.3 \pm 0.3$ and 5.9 ± 0.3 mb/sr unit(GT) at 130 and 170 MeV for the ^{40}Ca$(n,p)^{40}$K cross sections, respectively. This may be compared with $\hat{\sigma} = 5.5 \pm 0.2$ mb/sr unit(GT) at $E_p = 160$ MeV from the published ^{40}Ca$(p,n)^{40}$Sc result [2].

In Fig. 6, we show the multipole decomposed 170-MeV ^{40}Ca$(n,p)^{40}$K data spectrum at $\theta_{\mathrm{c.m.}} = 1.0°$ and the *extracted* $L = 0$ cross section. The 2^- state at $E_x = 0.8$ MeV, whose differential cross section is comparable to that of the 1^+ state at $E_x = 2.7$ MeV [1, 2], is not well recognized in this figure. This may be due to the hydrogen contamination in the target. To extrapolate to $q = \omega = 0$, the $L = 0$ cross sections were multiplied by

the factor

$$\left[\frac{\sigma^{\mathrm{DW81}}(q=0,\omega=0)}{\sigma^{\mathrm{DW81}}(\theta=0^{\circ},q,\omega)}\right]. \quad (4)$$

In our case the value of the expression in brackets is equal to 1, 1.25, and 3.25 at E_x = 0, 10, and 35 MeV, respectively. This correction presents a rather delicate situation in evaluating B(GT) values at higher excitations. Even small errors in the evaluation of the L = 0 differential cross sections get magnified by more than threefold at about 30-MeV excitation energy. Furthermore, the extracted L = 0 cross sections are susceptible to the choices of the 1p-1h configurations used to represent the transitions to the unbound region in the multipole decomposition analysis. Therefore we limit the discussion of our analysis only up to 15 MeV excitation energy.

We estimate that between E_x = 0 and 15 MeV, the sum of the L = 0 cross sections after extrapolation to q = 0 fm^{-1} are about 8.5 ± 0.5 and 9.0 ± 0.5 mb/sr from the multipole decomposed 130 and 170 MeV ^{40}Ca$(n,p)^{40}$K data, respectively. Thus, we estimate $\sum_{E_x=0}^{15\ \mathrm{MeV}} B(\mathrm{GT})$ values of 1.6 ± 0.1 and 1.5 ± 0.1 for the 130 and 170 MeV data, respectively. The uncertainties are just of statistical nature.

From the multipole decomposed spectrum of the 170 MeV ^{40}Ca$(n,p)^{40}$K data, we obtain σ_{GT} = 0.8 ± 0.1 and 1.0 ± 0.1 mb/sr for the proton groups at E_x = 2.7 and 4.3 MeV, respectively. With these cross sections and the $\hat{\sigma}$ given above for the 170-MeV ^{40}Ca$(n,p)^{40}$K reaction, we estimate B(GT) = 0.14 ± 0.02 and 0.17 ± 0.02 for the two proton groups located at E_x = 2.7 and 4.3 MeV in the (n,p) data, respectively. The B(GT) for these two states represent about 20% of the $\sum_{E_x=0}^{15\ \mathrm{MeV}} B(\mathrm{GT})$ in the 170-MeV ^{40}Ca$(n,p)^{40}$K data. These values are in good agreement with B(GT) = 0.21 ± 0.04 and 0.20 for the E_x = 2.7 and 4.3 MeV states from the 160-MeV ^{40}Ca$(p,n)^{40}$Sc measurements.

This large B(GT) value from the multipole decomposed ^{40}Ca$(n,p)^{40}$K data up to 15 MeV excitation energy can only be explained with 2p-2h and higher ground state correlations in which $0^+ \rightarrow 1^+$ transitions are not blocked. It has been shown [6, 7] that the occupation probabilities N_{nlj} of the proton single-particle orbits in ^{40}Ca, that are estimated using the dispersive mean field, for $1f_{7/2}, 1d_{3/2}, 2s_{1/2}, 1d_{5/2}, 1p_{1/2}, 1p_{3/2}$, and $1s_{1/2}$ subshells are 0.14, 0.85, 0.87, 0.88, 0.91, 0.92, and 0.93, respectively. The single-particle orbits that lie in (above) the Fermi sea are not fully occupied (are not entirely empty) because of the residual NN interaction. The N_{nlj} of 0.85, i.e., 85% occupancy, for the $1d_{3/2}$ subshell alone *indicates* that 2p-2h and higher excitations are possible. Transitions involving other subshells would undoubtedly *produce* additional GT transitions. Adachi *et al.* [4] have used a second order perturbation calculation

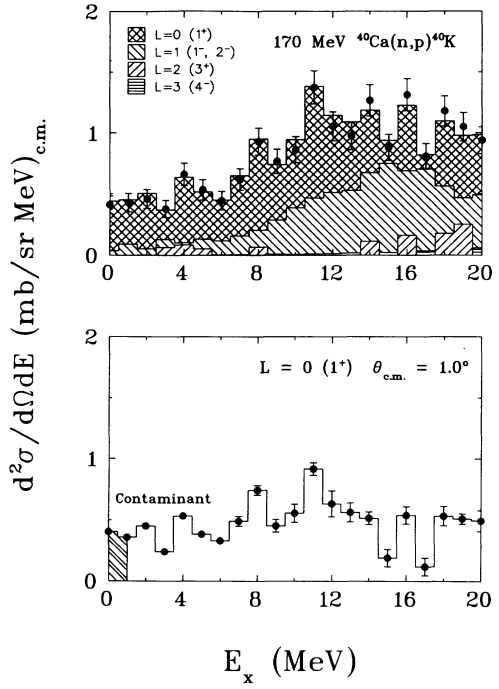

FIG. 6. The multipole decomposed 170-MeV ^{40}Ca$(n,p)^{40}$K spectrum at $\theta_{\mathrm{c.m.}}$ = 1.0°, and the isolated plot of the L = 0 cross section. Hydrogen contamination is shown in shaded area.

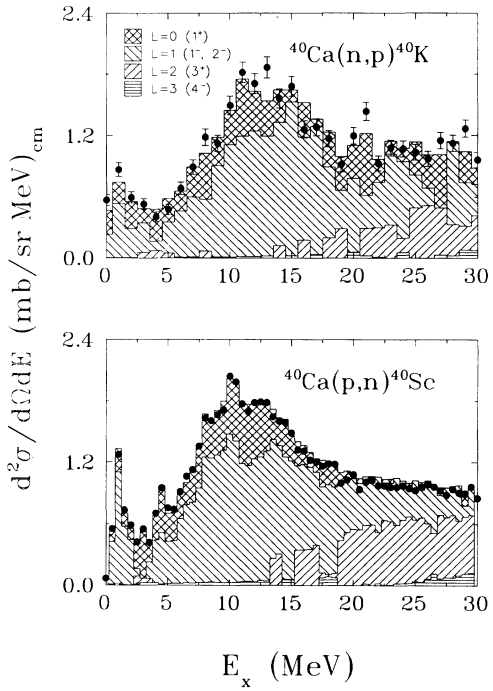

FIG. 7. The multipole decomposed 170-MeV ^{40}Ca$(n,p)^{40}$K and the 160-MeV ^{40}Ca$(p,n)^{40}$Sc [2] spectra at $\theta_{\mathrm{c.m.}}$ = 5.2°. The (p,n) and (n,p) data were multipole decomposed with excitation energy bins of 0.5 and 1 MeV, respectively. The same choices of $\sigma(\theta)^{J^\pi}$'s were used in the multipole decomposition analysis of both spectra. In both (n,p) and (p,n) spectra at this angle, we observe almost the same amount of GT strength and nearly the same higher L transfer contributions with a good overall agreement between the two spectra.

with Bertsch and Hamamoto interaction [5] to *estimate* the GT strength that extends out to high excitation energies. The contribution of the central (V_C) and tensor (V_T) terms in the interaction to the GT strength values in ^{40}Ca are estimated to be substantial: $\sum_{E_x=0}^{\sim 20\ \mathrm{MeV}} B(\mathrm{GT})$ = 0.825 and 1.786 assuming the perturbation interaction to be the central (V_C) and tensor (V_T) interactions of Bertsch and Hamamoto, respectively. If the calculations are extended to include $J^\pi = 1^+$ states up to about 60 MeV, the value increases to $\sum_{E_x=0}^{\sim 60\ \mathrm{MeV}} B(\mathrm{GT}) = 1.26$ and 4.66 from V_C and V_T terms, respectively. As pointed out by the authors, these results are highly dependent upon the choice of the interaction, and it remains to be seen how they would change if one calculates with other realistic interactions.

A similar situation has been reported in the analysis of the ^{16}O$(n,p)^{16}$N data [39] measured at 298 MeV. The ^{16}O ($N = Z = 8$) target is also a doubly magic nucleus, and in the independent-particle shell model it is described by the $1s_{1/2}, 1p_{3/2}, 1p_{1/2}$ double-closed shells. This description excludes $L = 0$ transitions because it forces the charge exchange transition into the *s-d* shell orbits. The nonzero GT strengths observed in the ^{16}O$(n,p)^{16}$N are due to particle-hole correlations in the ground state and $4\hbar\omega$ [40] nuclear shell model calculations seem to reproduce the observed GT strengths to a reasonable level. The $\sum_{E_x=0\ \mathrm{MeV}}^{40\ \mathrm{MeV}} B_{\mathrm{GT}}$ reported in Ref. [40] is about 0.6 unit. It is interesting to note that Adachi *et al.* [4] also report a value of 0.6 unit for the GT strength in ^{16}O, assuming only the central V_C term for the perturbation interaction and including 1^+ states up to 80 MeV of excitation. The separate contribution of the tensor interaction is 3.18 units for the GT strength.

It would be interesting to obtain the energy distribution of the calculated GT strength in ^{40}Ca and to compare with the empirical results shown in Fig. 6 as was done in Refs. [39,40] for the ^{16}O nucleus. The present ^{40}Ca$(n,p)^{40}$K results indicate good agreement for the GT strength observed in the (p,n) reaction to the 2.7 and 4.3 MeV states. We also have done a multipole decomposition to the 160-MeV ^{40}Ca$(p,n)^{40}$Sc data [2] (see Fig. 7). We have obtained $\sum_{E_x=0\ \mathrm{MeV}}^{15\ \mathrm{MeV}} B_{\mathrm{GT}} = 1.7 \pm 0.1$, which is in very good agreement with the 1.6 ± 0.1 value obtained in the present ^{40}Ca$(n,p)^{40}$K analysis.

C. Dipole strength distribution in the ^{40}Ca$(n,p)^{40}$K reaction

As indicated in the above section, the GT (L = 0) strength in spin-saturated nuclei, such as ^{40}Ca, is strongly suppressed. Thus, these nuclei are ideal cases to study the dipole and spin-dipole ($L = 1$) giant resonances. As such, in recent years several studies have been published. The excitation of the GDR is uniquely determined in photonuclear reaction and has been studied by Ahrens *et al.* [16]. Several authors report on the excitation of the GSDR observed in ^{40}Ca(p,p') [17,41–44] and ^{40}Ca$(\vec{p},\vec{p}')$ [18] reactions at intermediate energies. Horen *et al.* [17] have compared the spin-dipole cross sections obtained from the 500 MeV ^{40}Ca(p,p') reaction with the charge exchange ^{40}Ca$(p,n)^{40}$Sc cross sections obtained at 160 MeV [2]. The results appear to be in reasonable agreement.

The observed centroid of the GSDR is about 3 MeV below the centroid of the GDR estimated from the ^{40}Ca(γ,n) results [16]. An analysis of the present data, indicates a separation of about 2–3 MeV, which is in good agreement with the above value. This analysis is reported in Ref. [21].

In Fig. 7 we present the multipole decomposed 170 MeV ^{40}Ca$(n,p)^{40}$K and 160 MeV ^{40}Ca$(p,n)^{40}$Sc spectra at $\theta_{\mathrm{c.m.}} = 5.2°$. The (p,n) data had better energy resolution than the ^{40}Ca$(n,p)^{40}$K data, and therefore we performed a multipole decomposition with excitation energy binning of 0.5 MeV. Consequently, the 2^- state at $E_x = 0.8$ MeV is better *recognizable* in the ^{40}Ca$(p,n)^{40}$Sc data. Furthermore, in the (p,n) data, we observe somewhat more detailed structure of the $L = 1$ excitation, and the higher multipole transfers are better represented in a sense that smaller uncertainties were obtained in the multipole decomposition analysis than in the (n,p) data. However, the overall agreement between the multipole decomposed spectra of the ^{40}Ca$(n,p)^{40}$K and ^{40}Ca$(p,n)^{40}$Sc data at this angle is quite reasonable. We observe almost the same amount of GT strength and nearly the same higher L transfer contributions below 20 MeV excitation energy.

Assuming a simple 1p-1h model, we have used the shell model code OXBASH to calculate the excitation energies and OBDME for the dipole and spin dipole states in ^{40}Ca. The DW81 calculations were then carried out for each excited state. The 2^- state at $E_x = 0.8$ MeV was easily distinguishable in the multipole decomposed spectra for the 170-MeV ^{40}Ca$(n,p)^{40}$K data at various angles. In Fig. 8 we present the angular distribution for the proton group observed at $E_x = 0.8$ MeV determined from the multipole decomposed spectra. The curve shown in this figure is a $J^\pi = 2^-$, assuming a pure $1f_{7/2}$-$1d_{3/2}^{-1}$ DWIA

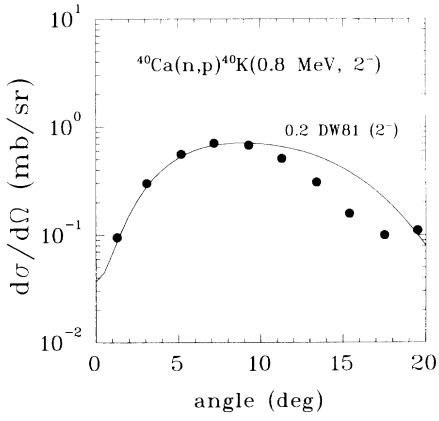

FIG. 8. Angular distribution for the proton group observed at $E_x = 0.8$ MeV with 170 MeV incident neutrons for the ^{40}Ca$(n,p)^{40}$K reaction. The curve shown is a $1f_{7/2}$ particle–$1d_{3/2}$ hole and $J^\pi = 2^-$ DWIA calculation normalized by 0.2.

calculation normalized by a factor of 0.2. A good agreement is observed. The same normalization factor was used to describe the angular distribution of the 2^- state at $E_x = 0.8$ MeV in the 160 MeV ^{40}Ca$(p,n)^{40}$Sc data. The $M2$ strength for the analogous ^{40}Ca$(e,e')^{40}$Ca(8.43 MeV) transition has been measured by Richter *et al.* [45]. A value $B(M2)\uparrow = (235 \pm 20)\mu_N^2$ fm^2 is quoted for the transition. A pure $1f_{7/2}$-$1d_{3/2}^{-1}$ transition yields a result of about 6 times larger, $B(M2)\uparrow = 1495\mu_N^2$ fm^2 [2]. Thus in the absence of significant orbital contribution to $B(M2)\uparrow$, this normalization is consistent with the normalization of 0.2, between the calculated and measured (n,p) cross sections.

In Fig. 9 we show the integrated sum of the $L = 1$, 1p-1h cross sections from DW81 calculations for $E_n = 170$ MeV at $\theta_{\rm c.m.} = 7.2°$ and that of the multipole decomposed spectrum for the 170 MeV ^{40}Ca$(n,p)^{40}$K data at the same angle. The calculations use OBDME from a simple 1p-1h model, and include 21 $(J^\pi = 0^-, 1^-, 2^-)$ states for the $L = 1$ transfer between $E_x = 0.8$ and 16.55 MeV. In Fig. 9 only about a fifth of the cross section calculated with the 1p-1h wave functions is empirically observed up to 16 MeV. This factor of 0.2 is the same normalization that we used to compare the calculated and measured cross sections of the $J^\pi = 2^-$ state at $E_x = 0.8$ MeV. This may be compared with the ^{16}O(n,p) study [39] in which approximately 50% of the cross section, also calculated with a 1p-1h shell model, is experimentally observed. In Fig. 10 we present the calculated dipole cross sections at $q \sim 0.4$ fm^{-1}, close to the $L = 1$ peak location, for the ^{40}Ca$(n,p)^{40}$K reaction at $E_n = 95$ and 170 MeV. In this figure, the excited states corresponding to $J^\pi = 0^-, 1^-$, and 2^- states are shown with dot-dashed, dashed, and solid lines, respectively. The calculated cross sections are shown in Gaussian distribution with 1 MeV full width at half maximum to match the energy resolution of the experimentally observed spectra. In Fig. 11 these calculations are superimposed on

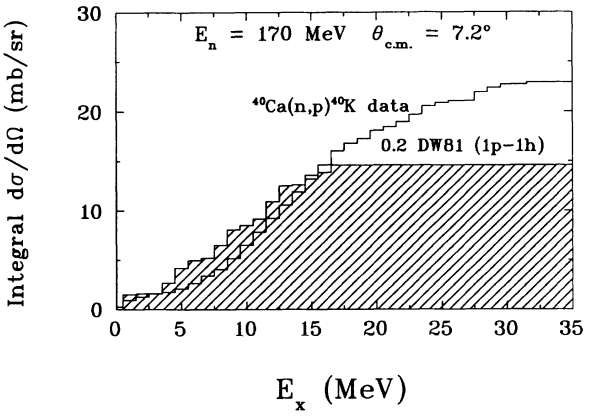

FIG. 9. Running sum of the $L = 1$ differential cross section $(d\sigma/d\Omega)$ obtained from the multipole decomposed spectrum at 170 MeV and $\theta_{\rm c.m.} = 7.2°$. Calculated cross sections are normalized by a factor of 0.2 and are shown in the shaded area.

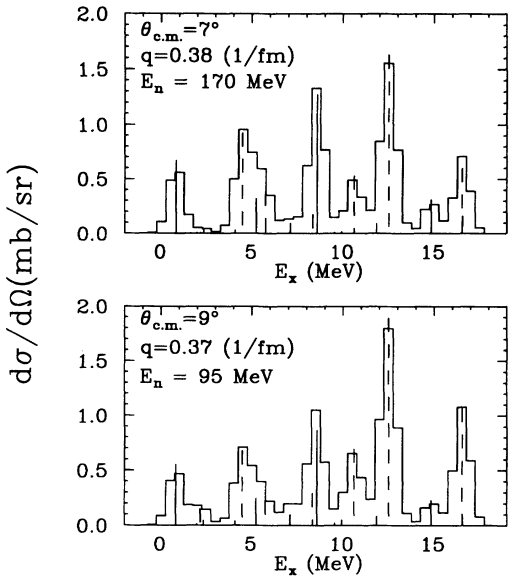

FIG. 10. The calculated 1p-1h dipole differential cross sections at $q \sim 0.4$ fm^{-1}, for the ^{40}Ca$(n,p)^{40}$K reaction at $E_n = 95$ and 170 MeV. The excited states corresponding to $J^\pi = 0^-, 1^-$, and 2^- states are shown with dot-dashed, dashed, and solid lines, respectively. Three $J^\pi = 0^-$ cross sections are very small and cannot be easily seen in this figure. The largest 0^- cross section (0.159 mb/sr) is calculated at $E_x = 16.55$ MeV for the 170 MeV ^{40}Ca$(n,p)^{40}$K, and all others are less than 0.05 mb/sr.

$L = 1$ cross sections from the multipole decomposed 170-MeV ^{40}Ca$(n,p)^{40}$K data at $\theta_{\rm c.m.} = 5.1°$. The simple 1p-1h model *predicts* spin-dipole strength only up to 16.55 MeV. The observed $L = 1$ strength seems to extend to about 30 MeV in excitation energy. These simple 1p-1h calculations, which are normalized by a factor of 0.2 to *resemble* the experimentally observed data, show a fairly good agreement with the observed $L = 1$ dipole excitations. The 1p-1h results seem to predict reasonably well the shape and location of $L = 1$ cross sections

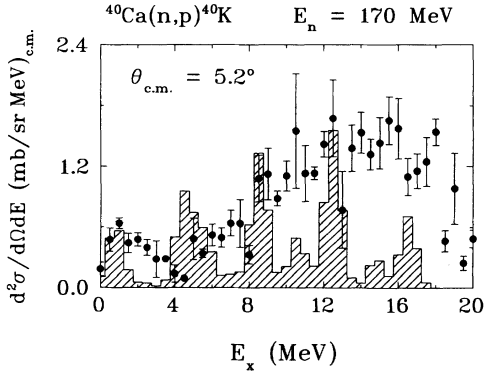

FIG. 11. Normalized 1p-1h DWIA differential cross sections are superimposed on the $L = 1$ spectrum from the multipole decomposed 170 MeV ^{40}Ca$(n,p)^{40}$K data at $\theta_{\rm c.m.} = 5.2°$.

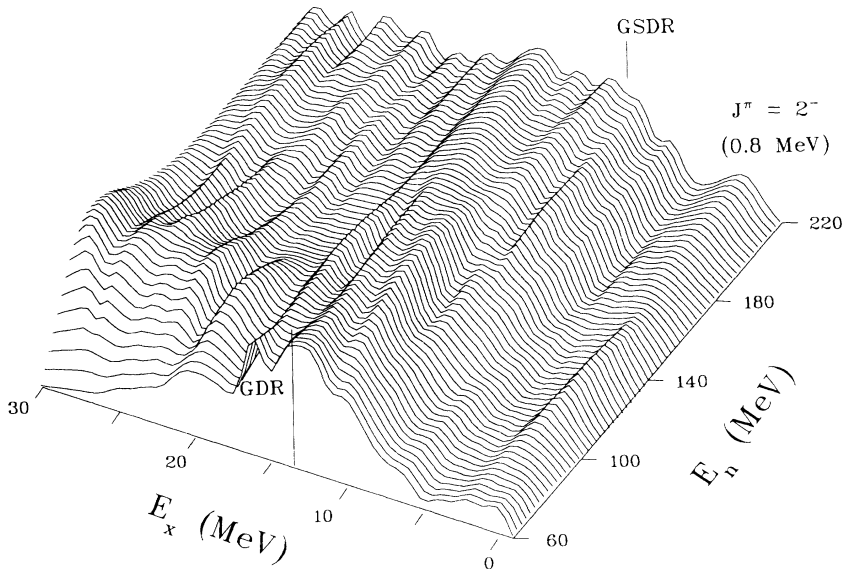

FIG. 12. 3D plot (E_x, E_n, $d^2\sigma/d\Omega\,dE$) of ^{40}Ca$(n,p)^{40}$K data at $\theta_{\rm lab} = 7°$. A smooth increase in strength is observed for the 2^- state located at $E_x = 0.8$ MeV with increasing neutron energy. The strength of the lower part of the $L = 1$ dipole resonance at approximately $E_x \sim 13$ MeV appears to increase with neutron energy, consistent with its 2^- character and the energy dependence of the spin-flip and non-spin-flip nature of the $L = 1$ resonance.

below $E_x = 16.55$ MeV. A more sophisticated calculation with larger p-h configurations show the spreading of the spin dipole strength to higher excitation energies. Specifically, Wambach, and Unkelbach [46] have shown that DWIA calculations with a "second random-phase-approximation" (SRPA), which includes 1p-1h as well as 2p-2h excitations, produce better agreement with spin excitations in the (p,p') [18] reaction.

In Fig. 12 we present a 3D plot of (E_x, E_n, $d^2\sigma/d\Omega\,dE$) for the ^{40}Ca$(n,p)^{40}$K data at $\theta_{\rm lab} = 7°$. As the neutron energy increases above 110 MeV, we observe the GSDR to have a very distinct peak that is well separated from the GDR. On a relative scale, the upper excitation energy region ($E_x \geq 12$ MeV) is more strongly populated at the lower beam energies than the lower excitation energy region. This also can be seen in Figs. 3 and 5 between the 95 and 170 MeV ^{40}Ca$(n,p)^{40}$K spectra. The strength of the spin-flip 2^- state at $E_x = 0.8$ MeV handsomely increases with the incident neutron energy. Calculated transitions to states with $J^\pi = 1^-$ may have contributions from spin-transfer ($\Delta S = 1$) as well as non-spin-transfer ($\Delta S = 0$) components. This creates difficulty in separating how much of the observed $\Delta J^\pi = 1^-$ transition strength belongs to the GDR or GSDR [46,47]. On the other hand, transitions to either 0^- or 2^- states are pure GSDR transitions. Thus the overall increase in the 2^- state strength (see Fig. 10) with increasing beam energy makes the GSDR more prominent at higher beam energies.

As discussed above, for ^{40}Ca the GDR is uniquely excited in the (γ,n) reaction [16] while the GSDR has been studied with the (p,p') reaction [17] at 500 MeV. For qualitative comparisons, we present in Fig. 13 the arbi-

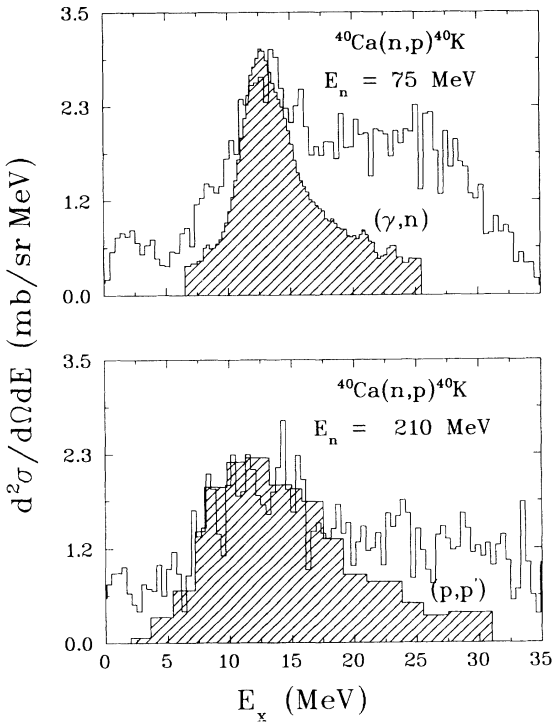

FIG. 13. Qualitative comparison of the 75 MeV (210 MeV) ^{40}Ca$(n,p)^{40}$K spectra (not multipole decomposed) at $\theta_{\rm lab} = 5°$ and GDR (GSDR) from (γ,n) [500 MeV (p,p')] data. Arbitrarily normalized GDR$^{(\gamma,n)}$ and GSDR$^{(p,p')}$ spectra are superimposed on the present (n,p) results. Both GDR$^{(\gamma,n)}$ and GSDR$^{(p,p')}$ are shifted by −7 MeV in E_x. A fair overall agreement is observed in this comparison.

trarily normalized GDR$^{(\gamma,n)}$ and GSDR$^{(p,p')}$ spectra superimposed on our (n,p) results at $\theta_{\rm lab} = 5°$ for $E_n = 75$ and 210 MeV, respectively. The 75-MeV ^{40}Ca$(n,p)^{40}$K data look very much like the GDR$^{(\gamma,n)}$ in the excitation energy region between 10 and 20 MeV. The obvious presence of excitation of some spin-dipole states in the 75 MeV ^{40}Ca$(n,p)^{40}$K data should account for the difference found in the $E_x = 5$ to 10 MeV region. We also observe a good agreement between the 210-MeV ^{40}Ca$(n,p)^{40}$K data and the spin-dipole spectrum obtained at the 500-MeV ^{40}Ca(p,p') reaction [17]. These comparisons help support the argument that a considerable portion of the dipole strength at lower beam energies is from the GDR, whereas the GSDR is more prominent at higher beam energies.

D. Quasifree scattering contribution

At intermediate nucleon energies the nuclear response at small momentum transfers ($q < 1$ fm^{-1}) is dominated by giant resonances of low multipolarities ($L = 0$, 1, 2). At larger momentum transfer the main characteristic of the inclusive spectra is a broad peak at energy transfer $\omega \sim q^2/2M$, where M is the nuclear mass. The individual giant resonances are not strongly excited. The energy transfer for the broad peak corresponds to the kinematics for NN scattering from a nucleon at rest and the width of the peak is attributed to Fermi motion of the struck nucleon. This peak is usually referred to as the quasifree (QF) peak. We have observed this peak in the ^{40}Ca$(n,p)^{40}$K reaction at energies above 150 MeV (see Fig. 14). Recently there has been interest in the location of this peak and in the evaluation of the observed cross section. Horowitz and Murdock [48] use a relativistic approach to estimate the QF cross section. However, experimental support for the relativistic description of QF scattering has mainly been confined to analyzing power or induced polarization [49]. We compare the present cross-section data to the nonrelativistic model of Brieva and Love [23]. Their code based on an interacting Fermi-gas model, and the following assumptions to calculate the inclusive QF scattering cross section: (1) eikonal plane waves for initial and final states, (2) nuclear matter density for target structure, as derived from electron scattering data, (3) uncorrelated polarization propagator and absorption for particle states, (4) effective NN force such as Franey and Love interaction, (5) finite size effects in a local-density approximation, and (6) relativistic kinematics. In Fig. 14, we present the calculated differential cross section normalized by 0.75 at $\theta_{\rm lab} = 25°$ as compared with the data. The location of the QF peak calculated with Brieva's code is at the free NN kinematic energy. A shift of 14 MeV was needed in the calculation to match the location of the observed QF peak. The calculation seems to indicate that below 15-MeV excitation energy, the QF contributions are rather small. A similar agreement is observed at higher angles not presented here. It may be noted that in Fig. 14, above 60 MeV of excitation, the measured cross section is higher than the calculation. To some extent this may be an artifact of the data that have been binned in a 2° scattering angle interval; however, calculations taking this into account did not show a much better agreement than the one presented in Fig. 14. A calculation done with the

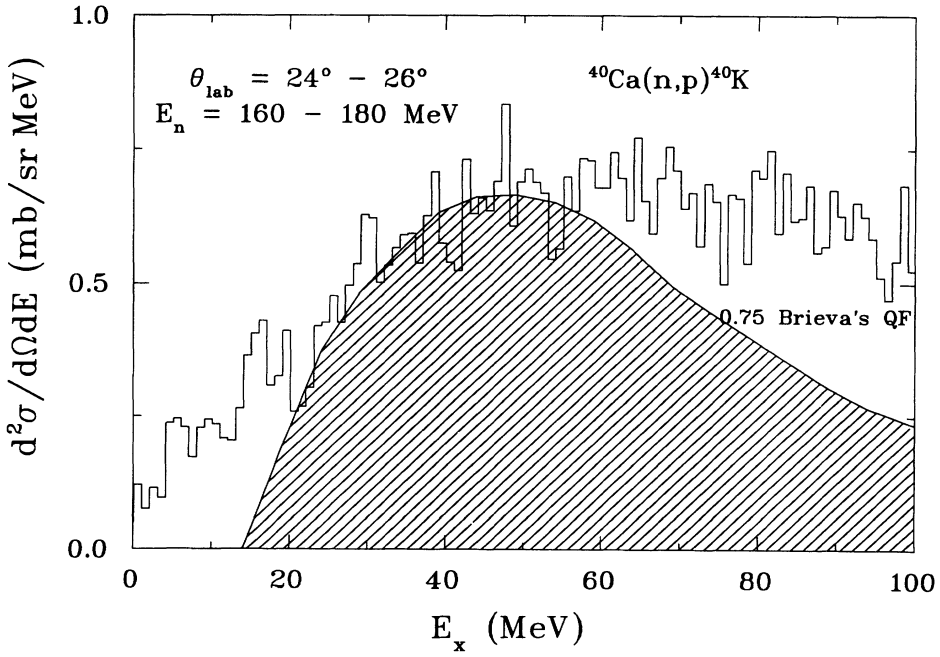

FIG. 14. The QF cross sections from the calculations of Brieva [23] for the 170-MeV ^{40}Ca$(n,p)^{40}$K reaction at $\theta_{\rm lab} = 25°$ superimposed on the observed excitation spectrum.

relativistic code of Horowitz improve the agreement only slightly when compared with the data.

IV. CONCLUSIONS

Double differential cross-section angular distributions were measured for the ^{40}Ca$(n,p)^{40}$K charge exchange reaction with a multitarget array and the LAMPF WNR spallation neutron source. With a "detection wall" made up of 15 CsI detectors, simultaneous measurements over incident neutron energies between 60 and 260 MeV were carried out covering the scattering angle range of $0° \leq \theta_{\rm lab} \leq 40°$.

A sizable GT strength [B(GT) = 1.6 ± 0.1] is observed below 15-MeV excitation energy in the ^{40}Ca$(n,p)^{40}$K data. A large GT strength has been previously reported in the (n,p) reaction on the light spin-saturated nucleus ^{16}O. The $\sum_{E_x=0\ \rm MeV}^{40\ \rm MeV} B_{\rm GT}$ for ^{16}O$(n,p)^{16}$N reaction reported in Refs. [39, 40] is about 0.6 unit. The implication of the observed GT strengths, whose value lie between the simple shell model prediction [B(GT) = 0] and a second-order perturbation calculation [4] [for ^{40}Ca, $\sum_{E_x=0}^{\sim 20\ \rm MeV} B$(GT) = 0.825 and 1.786 from V_C and V_T, respectively], is that *better* theoretical work is very much in need because the closed nuclei such as ^{16}O and ^{40}Ca are ideal for studying the correlations in nuclear ground state wave functions. In order to not only confirm the present findings but also to reduce the uncertainties related to B(GT) values, additional (n,p) measurements need to be made preferably at selected energies and momentum transfers. For the $L = 1$ excitations, the 1p-1h shell model calculations were performed with the OXBASH shell model code. Generated OBDME were then used in DWIA calculations. The results were reasonable in predicting the dipole distribution for the ^{40}Ca$(n,p)^{40}$K reactions.

ACKNOWLEDGMENTS

This project was supported in part by the National Science Foundation under Grants No. PHY-88-1020-03 and No. PHY-87-22008; the U.S. Department of Energy under Contracts No. W-7405-ENG-36 and No. DE-AC05-76ER01067.

[1] T. Chittrakarn *et al.*, Phys. Rev. C **34**, 80 (1986); J.W. Watson *et al.*, Phys. Lett. B **181**, 47 (1986).
[2] T.N. Taddeucci *et al.*, Phys. Rev. C **28**, 2511 (1983).
[3] N. Anantaraman *et al.*, Phys. Rev. Lett. **46**, 1318 (1981).
[4] S. Adachi *et al.*, Nucl. Phys. **A438**, 1 (1985).
[5] G. Bertsch and I. Hamamoto, Phys. Rev. C **26**, 1323 (1982).
[6] W. Tornow *et al.*, Phys. Rev. C **42**, 693 (1990).
[7] C.H. Johnson and C. Mahaux, Phys. Rev. C **38**, 2589 (1988).
[8] M. Macfarlane, Can. J. Phys. **65**, 626 (1987).
[9] P.E. Burt *et al.*, Phys. Rev. C **25**, 2805 (1982).
[10] W. Steffen *et al.*, Phys. Lett. **95B**, 23 (1980).
[11] W. Gross *et al.*, Phys. Lett. **84B**, 296 (1979).
[12] L.W. Fagg *et al.*, Phys. Rev. C **4**, 2089 (1971).
[13] R. Moreh *et al.*, Phys. Rev. C **25**, 1824 (1982).
[14] W.A. Sterrenberg *et al.*, Phys. Rev. Lett. **45**, 1839 (1980).
[15] C. Gaarde *et al.*, Nucl. Phys. **A422**, 189 (1984); C. Gaarde *et al.*, *ibid.* **A369**, 258 (1981).
[16] J. Ahrens *et al.*, Nucl. Phys. **A251**, 479 (1975).
[17] D.J. Horen *et al.*, Z. Phys. A **333**, 39 (1989).
[18] F.T. Baker *et al.*, Phys. Rev. C **40**, 1877 (1989); F.T. Baker *et al.*, *ibid.* **37**, 1350 (1988); C. Glashausser *et al.*, Phys. Rev. Lett. **58**, 2404 (1987).
[19] R. Schaeffer and J. Raynal, computer code DWBA70, Arizona State University, 1970 (unpublished); extended J.R. Comfort, computer code DW81, Arizona State University, 1984 (unpublished).
[20] M.A. Moinester, Can. J. Phys. **65**, 660 (1987).
[21] B.K. Park, Ph.D dissertation, Ohio University (1991).
[22] B.A. Brown *et al.*, The Oxford-Buenos-Aires-MSU Shell Model Code OXBASH, Michigan State University Cyclotron Laboratory Report 524, 1986.
[23] F.A. Brieva and W.G. Love, Phys. Rev. C **42**, 2573 (1990).
[24] P.W. Lisowski *et al.*, Nucl. Sci. Eng. **106**, 208 (1990).
[25] D.S. Sorenson, Ph.D. dissertation, University of California, Davis (1990).
[26] R.S. Henderson *et al.*, Nucl. Instrum. Methods **A257**, 97 (1987).
[27] J.L. Ullmann (unpublished).
[28] R.A. Arndt and L.D. Roper, Scattering Analysis Interactive Dial-in (SAID) program (SM88) (unpublished).
[29] A.G. Ling *et al.*, Phys. Rev. C **44**, 2794 (1991).
[30] R. Brun *et al.*, GEANT3 User's Guide, Data Handling Division DD/EE/84-1, 1987.
[31] J.L. Romero (unpublished).
[32] M.A. Franey and W.G. Love, Phys. Rev. C **31**, 488 (1985).
[33] P. Schwandt *et al.*, Phys. Rev. C **26**, 55 (1982).
[34] G. Bertsch, *The Practitioner's Shell Model* (North-Holland, Amsterdam, 1972); M. Carchidi *et al.*, Phys. Rev. C **34**, 2280 (1986).
[35] B.K. Park, Ohio University Report OU91-Accel-01 (unpublished).
[36] D.J. Millener and D. Kurath, Nucl. Phys. **A255**, 315 (1975).
[37] T.N. Taddeucci *et al.*, Nucl. Phys. **A469**, 125 (1987).
[38] J. Rapaport, in *Spin and Isospin in Nuclear Interactions, Telluride, Colorado, 1991*, edited by S. W. Wissink, C. D. Goodman, and G. E. Walker (Plenum, New York, in press).
[39] K.H. Hicks *et al.*, Phys. Rev. C **43**, 2554 (1991).
[40] W.C. Haxton and Calvin Johnson, Phys. Rev. Lett. **65**, 1325 (1990).
[41] J. Lisantti *et al.*, Phys. Rev. C **39**, 568 (1989).
[42] J. Lisantti *et al.*, Phys. Rev. C **40**, 211 (1989).
[43] D.J. Horen *et al.*, Phys. Lett. **99B**, 383 (1981).
[44] D.J. Horen *et al.*, Phys. Lett. **95B**, 27 (1980).
[45] A. Richter Nucl. Phys. **A374**, 177c (1982).
[46] J. Wambach, KFA-IKP(TH)-1991-22.
[47] N. Auerbach and A. Klein, Phys. Rev. C **30**, 1032 (1984).
[48] C.J. Horowitz and D.P. Murdock, Phys. Rev. C **37**, 2032 (1988).
[49] O. Häusser *et al.*, Phys. Rev. C **43**, 230 (1991).
[50] B.K. Park (unpublished).